CHINESE JOURNAL OF GEOPHYSICS Vol.49, No.3, 2006, pp: 657∼670

STUDY OF EARTH'S GRAVITY TIDE AND OCEAN LOADING CHARACTERISTICS IN HONGKONG AREA

SUN He-Ping[1] HSU House[1] CHEN Wu[2] CHEN Xiao-Dong[1]
ZHOU Jiang-Cun[1] LIU Ming[1] GAO Shan[2]

1 *Key Laboratory of Dynamical Geodesy, Institute of Geodesy and Geophysics, Chinese Academy of Sciences, Wuhan* 430077*, China*

2 *Department of Land Surveying and Geoinformatics, Hong-Kong Polytechnic University, Hung Hom, Knowloon, Hong Kong*

Abstract The tidal gravity observation achievements obtained in Hongkong area are introduced, the first complete tidal gravity experimental model in this area is obtained. The ocean loading characteristics are studied systematically by using global and local ocean models as well as tidal gauge data, the suitability of global ocean models is also studied. The numerical results show that the ocean models in diurnal band are more stable than those in semidiurnal band, and the correction of the change in tidal height plays a significant role in determining accurately the phase lag of the tidal gravity. The gravity observation residuals and station background noise level are also investigated. The study fills the empty of the tidal gravity observation in Crustal Movement Observation Network of China and can provide the effective reference and service to ground surface and space geodesy.

Key words Hongkong area, Tidal gravity, Experimental model, Ocean loading

1 INTRODUCTION

The Earth's gravity is a science studying the temporal and spatial distribution of the gravity field and its physical mechanism. Generally, its achievements can be used in many important domains such as space science, geophysics, geodesy, oceanography, and so on. The past researches have indicated that the Earth is a very complex and nearly layered ellipsoid body. The substances in each layer are totally different, they may be elastic, anelastic, plastic or even liquid status. The gravity field includes Earth's gravitational force and the inertial centrifugal force caused by self rotation of the Earth[1]. In addition, it also includes the gravitational force caused by the Sun, the Moon and other celestial bodies, as well as the inertial force related to the translation movement of the Earth's center. The resultant force of the later ones is usually called tidal generating force. The inner and outside appearance of the solid Earth is changing with time periodically under the action of the tidal generating force. These phenomena are traditionally called solid Earth's tides (or Earth tides). The existence of the Earth tides induces the variation in various geophysical fields, such as gravity, tilt, strain and surface displacements and so on. The past studies have shown that the high-precision tidal gravity observation is an effective technique, which is different from the seismology method, to detect inner dynamics and to inverse the inner structure of the Earth. It can also provide powerful constraints to investigate the gravity changes caused by the Earth's free oscillation, the nearly diurnal free wobble (NDFW) of the Earth's liquid core, the translation oscillation of the Earth's solid core, the Earth's rotation, and so on. It is an important approach to explain the gravity variation induced by the surface mass flow, such as atmosphere, ocean, surface land water, it is also an important measure to detect various regional environmental influences[2∼4].

Since the geophysical year of 1957, the International Center for Earth Tides (ICET) has established several global profiles of the tidal gravity observations which are composed of more than 300 stations. These works acquired a large number of accurate tidal gravity parameters in many important areas and a lot of important achievements[5]. The study of the Earth tides has advanced to a new stage since the starting of the cooperation in the Global Geodynamics Project (GGP) in 1996[6].

E-mail: heping@asch.whigg.ac.cn

Hongkong area is a costal island in southern China, an important absolute gravity control point is located in this area. Therefore, it plays an important role in the gravity network of the national great scientific network to carry out gravity measurement, to obtain temporal and spectral characteristics of the gravity field and to obtain variation property of the ocean loading in this area. The mutual cooperative observation achievements in tidal gravity in Hongkong area under cooperation between the Institute of Geodesy and Geophysics, Chinese Academy of Sciences and the Hongkong Polytechnic University will be introduced in this paper. The main purpose of this work is to obtain the accurate tidal gravity parameters in order to provide the tidal gravity experimental model for the surface and spatial geodesy in this area. The suitability of the global ocean tidal models is also investigated. The temporal and spectral characteristics of the observed tidal gravity residual and station background noise are also analyzed by using air pressure and tidal gauge observations.

2 INSTRUMENTAL CALIBRATION AND DATA PREPROCESSING

2.1 Brief Introduction of the Observation

The observing station of the Earth tides locates in a half-underground room at the Hongkong Astronomy Observatory (HKAO), 132A, Mi-Deng Avenue in Hongkong. The observation room is about 4m from ground surface and the perennial room temperature is about 23°C. There are also long-period seismograph, short-period seismograph, strong-motion seismograph and other instruments installed in the same room. The LCR-ET20 gravimeter is successfully installed onto the observation pillar, same pillar as the national absolute gravity base point, in August 2002. The observation pillar is connected with the base rock and separated from the surroundings with the shock insulation slot. The entrance of the observing room and observation pillar are shown in Fig. 1.

Fig. 1 Entrance of observation room (a) and sketch map of observation pillar (b)

Before starting the observation of tidal gravity, the level positions of the gravimeter are carefully checked with tilting method. The readings of the horizontal and vertical water bubble are calibrated and the recording sensitivity of the data acquisition system is determined by using a displacement technique. The LCR-ET20 gravimeter was introduced from USA in 1981 and it is a kind of mechanical feedback spring gravimeter. An electrical feedback system and a DOS data acquisition system were installed under a cooperation project with the Institute of Geodesy, Darmstadt University in Germany in 1989[7]. A new digital data acquisition system compiled with Visual Basic 6.0 in Windows 98/2000 system developed by Liu et al was installed in the year 2000. In addition, some peripheral equipments such as the A/D converter and so were replaced, the gravimeter was updated in both software and hardware[8]. Matching with the gravimeter, a device to observe air pressure is equipped. The data acquisition system records automatically the 1s sampling gravity and air pressure readings, and they are saved on to computer hard and soft disks respectively. The output sampling rate can be controlled easily by manual, and the sampling resolution of the gravimeter is 0.01 mV. The working staff checks the instrument condition everyday, and the data are analyzed and preprocessed in time in order to trace data quality.

The data period used in this study is from August 23, 2002 (03:42′00″) to December 18, 2003 (06:54′00″), in total 483 days. Because the Hongkong government has a rigid policy for setting up the permanent GPS observing point and establishing an antenna, we waited a period for getting the permission. As a consequence, we cannot correct the computer time with real GPS signal during very beginning. In order to correct the computer time, a temporary manual GPS receiver was used. Finally, a GE-II GPS synchronous satellite timer was installed, then the time problem of the data acquisition system was resolved completely on November 18, 2002. Inside the GE-II GPS synchronous satellite timer, there is a high-precision temperature compensatory quartz crystal, it assures a time error less than 1s during 10 days without receiving the GPS signal. The temporary manual GPS antenna is taken outside of the observation room for a while every week for receiving the GPS signal to renew the synchronous clock, and for keeping the timer accuracy within the permitted precision range of the observation analysis.

The following numerical analysis demonstrates that accurate tidal gravity parameters are achieved due to taking the effective remedial measures and installing the GE-II GPS synchronous satellite timer. There exist recording failures caused by the computer virus and one mistake in correcting manually the GPS timer at the very beginning period of the observation. Hence there are in total two relatively large recording gaps, i.e., (1) from October 2, 2002 (00:00′00″) to October 21, 2002 (07:18′20″) and (2) from November 7, 2002 (00:00′00″) to November 18, 2002 (07:06′20″). Additionally, during the instrument working period, the data acquisition system produced a date error, which was corrected effectively in the data preprocessing.

2.2 Gravimeter Calibration

Because the direct output of the gravimeter is the change in voltage, therefore the first work should be done is to determine the scale value of the gravimeter (also named calibration factor), i.e., the corresponding gravity value to unit voltage. Once having the instrument scale value, the change in the gravity value with time according to the variation of the output voltage of the gravimeter can be obtained easily[9]. The calibration of the LCR-ET20 spring gravimeter was done in Wuhan for several times. However, due to the nonlinear creep of the instrumental spring and secular drift, the original calibration value is changed, hence it cannot suit the requirement at new station. Although this kind of change is slight, it is still very important in determination of the high-precision tidal parameters, especially to the determination of the phase lags.

The scale value is determined by using the "reading wheel method". Usually when sellig the instrument, the manufacturer provides us with a preliminary mechanical scale value C_0, i.e., the corresponding gravity value to one circle of the reading wheel. Hence, if we know the relation between the reading number of the wheels and the changes in output voltage, then the relation between the voltage change in instrument output and gravity value will then be determined. The detail procedure is described as follows. Firstly we record a voltage value v_1 at time t_1, then turn 1000 circles of the reading wheel in a fixed direction, which is equivalent to give manually a voltage change of 3.8 volts, and record a voltage value v_2 at time t_1. Finally we turn 1000 circles of the reading wheel in the inverse direction, to let the reading wheel back to the original place, and record a voltage value v_3 at time t_3. Considering that it takes only several minutes to finish the whole procedure, the nonlinear influence due to the tide and other environmental factors can be neglected, i.e., a linear relation among the observed values at t_1, t_2 and t_3 can be regarded. Thus the observed voltage value at t_2 can be obtained by using linear interpolation between the value v_1 and v_3 at t_1 and t_3 respectively, the formula takes the form as $v_2' = v_1 + (v_3 - v_1)(t_2 - t_1)/(t_3 - t_1)$. If $(t_2 - t_1)$ and $(t_3 - t_2)$ can be set to equal each other during the calibration procedure, then the v_2' will be the average value of v_1 and v_3. The real calibration factor of the instrument is equal to the ratio of the gravity changes corresponding to 1000 circles of reading wheel and the residual that the observed value v_2 at t_2 minus v_2'. The formula takes the form as $C = 1000 \times C_0/(v_2 - v_2')$. After finishing one calibration cycle, the next calibration will be done in several minutes later after the instrument returns back to its initial status, several cycles can be done based on the working requirement.

In order to check the stability of the gravimeter calibration factor, two calibration campaigns are carried out at the beginning and the ending period of the tidal gravity observation period in Hongkong. In the first

calibration campaign, 7 times of calibration along the positive and negative directions are done respectively (see Fig. 2a). One scale value can be determined for each calibration. The average of all scale values is taken as the one in first calibration campaign. Using the same procedure, 4 times of calibration along the positive and negative directions are carried out before the end of observation (see Fig. 2b). Also the average value of all scale values is taken as the one in second calibration campaign. The numerical results show that the difference obtained between two calibration campaigns is slight, it means that the instrumental scale value is comparatively stable during the Hongkong observation period, it is influenced slightly by environmental perturbations. As a consequence, the final scale value of the instrument is taken as the average value obtained in two campaigns, i.e., $42.685\pm0.004\times10^{-8}\mathrm{m\cdot s^{-2}/V}$. Comparing with the scale value determined at the Jiufeng/Wuhan Geodynamical Observation Station in 2000, the difference is 0.6%. This denotes that the instrumental scale value is changing with time, therefore, it is necessary to carry out the calibration[9].

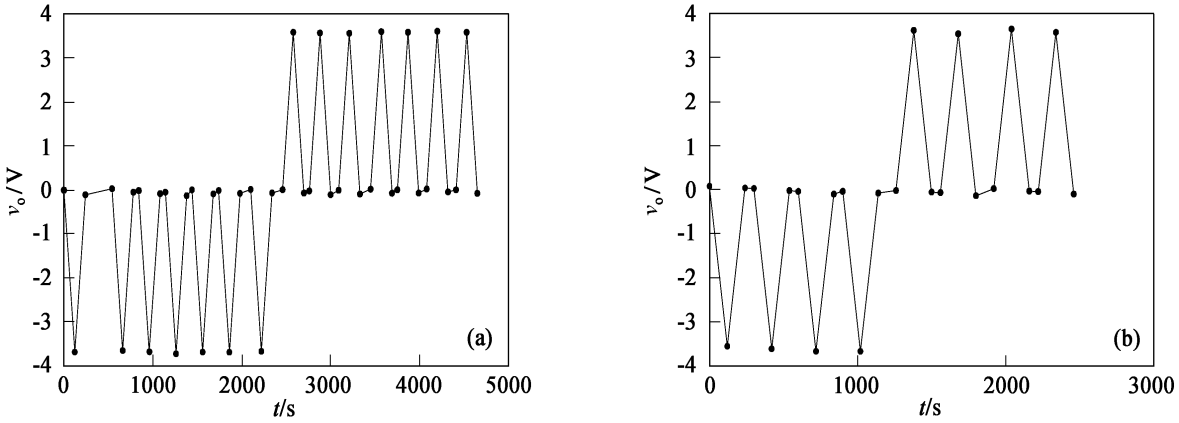

Fig. 2 Sketch of the first calibration on August 23, 2002 (a) and secondary calibration on December 18, 2003 (b)

In order to record efficiently the temporal variation characteristics of the tidal gravity, an output range of the gravimeter is set up as ±4V according to the linear measuring range of the instrument. An automatic step correction device is installed simultaneously onto the gravimeter in order to ensure the gravity signal inside the setting range[8]. The instrument will turn automatically the "reading wheel" to create a step in the recording once the output signal is outside this setting range. The data acquisition system records automatically the step values, which can be easily corrected manually during the data preprocessing.

Because the barometer output equipped together with gravimeter is also the change in voltage, the calibration work is needed too. Based on the calibrated standard air pressure data in November 2003 provided by the HKAS, firstly the local time is converted to the universal one (UTC), then the scale value of the air pressure is calculated with linear regression by comparing two time series after getting rid of the erroneous signals exceeding three times of the mean square error (MSE). The determined scale value is 121.197 hPa/V. Using this scale value to calibrate the air pressure observations, the change in station air pressure is then obtained for further tidal gravity analysis.

2.3 Data Preprocessing

After having the scale value, the preprocessing of the change in tidal gravity and air pressure can be carried out now. By using unique filters in data preprocessing, the 1m sampling data are obtained from 1s sampling ones. By further filtering process, the 1h sampling observations of the original tidal gravity $G(t)$ and the change in station air pressure $P(t)$ are obtained respectively (see Fig. 3). The 1 minute sampling data are preprocessed by using the Tsoft data preprocessing software recommended by the ICET[10]. The "remove-restore technique" is adopted in the data preprocessing, that is to say, to get the observed tidal gravity residuals by removing the theoretical tidal gravity signals. Then by using a visual man-machine interface, the preprocessing is carried, and various perturbation signals are corrected, including the signals as of steps, gaps, spikes, earthquakes, and

so on. The air pressure correction is done using a theoretical atmospheric gravity admittance. Finally the first-preprocessed tidal gravity observations are achieved by restoring the theoretical synthesized signals removed at the beginning. The tidal gravity parameters for several main waves in Hongkong area are obtained by carrying out the harmonic analysis.

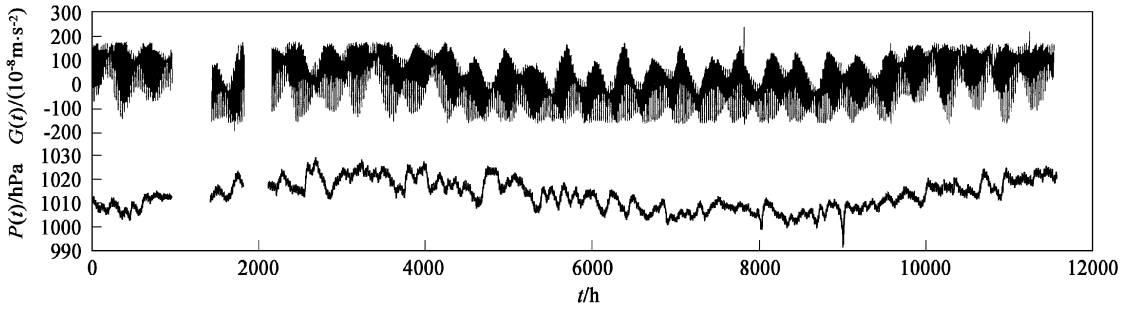

Fig. 3 Calibrated tidal gravity change and station air pressure variation

On the basis mentioned above, the synthesized tidal gravity signals are composed with the real tidal gravity parameters mentioned above. Repeating the above procedure, the tidal gravity observation residuals are obtained again by removing the synthesized tidal gravity signals. The regression analysis is carried out on the secondary tidal gravity residual and air pressure, by using the estimated regression coefficient, the air pressure correction is done. The harmonic analysis for the preprocessed and air pressure corrected tidal gravity observations is carried out, and then the final tidal gravity parameters in Hongkong area are obtained[11].

As a matter of fact, in order to carry out preprocessing conveniently and to ensure correctness in the procedure of modifying perturbation signals, the monthly data are preprocessed respectively. After all the monthly data are completed, all data files are connected into one data set. In order to avoid the filter edge effect, one more day's data in the beginning and in the end of each month are added during preprocessing. After having the 1m sampling data file, the 1h sampling data are obtained by applying the filtering process again. Finally, the 1h sampling corrected data are connected into one file in standard format[12]. The tidal gravity observations $G_{\rm c}(t)$ after correcting for various interferences and steps are shown in Fig. 4. From this figure, it can be seen that the long-term drift induced by the gravimeter spring creep is very obvious. Therefore, it is very important to deduct the drift with an appropriate method if an accurate estimation of the tidal gravity parameters is required. By using the 10-order polynomial fitting, the fitted long-term drift function $D(t)$ and the tidal gravity observations $G_{\rm ok}(t)$ after deducting the long term drift are given in Fig. 4.

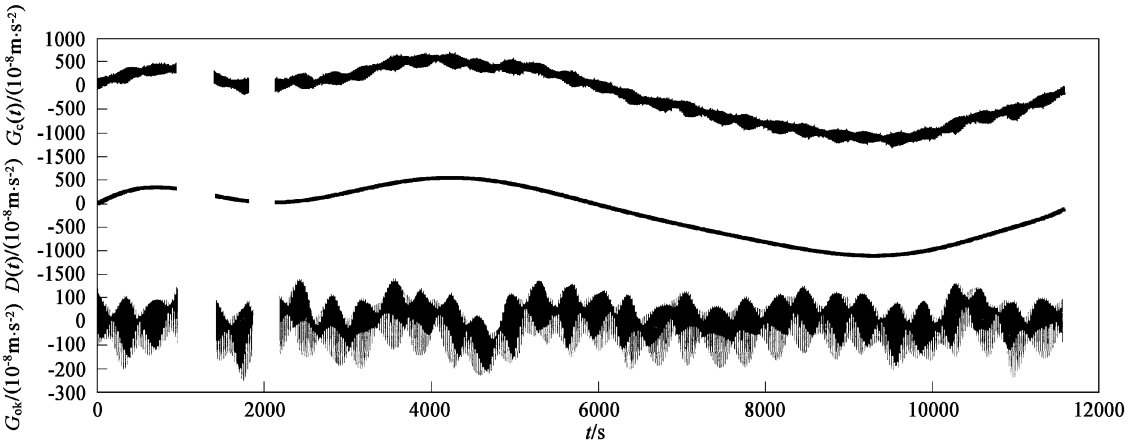

Fig. 4 Tidal gravity variation after correction of the steps and various disturbances $G_{\rm c}(t)$, fitted instrumental drift $G_{\rm or}(t)$ and tidal gravity change after correction of instrument drift $G_{\rm or}(t)$

2.4 Processing of Tide Gauge Data

In order to study the correlation between the station background noise and tidal gravity residual signals, we obtained the tidal gauge data from three stations, as of the Quarry Bay, ShekPik and Waglan Island from the HKAO. The tidal gauge stations provide us with the change in tidal height, the fundamental standard in height level used for the tide gauge recording is 14.6cm lower than the currently used Hongkong standard height level. The sampling rate of the tidal height data is 1h; and the unit is cm. The data period is from August 20, 2002 to December 31, 2003. In the same way as preprocessing the air pressure data, the local time is converted to Greenwich time. Fig. 5 shows the original change in the tidal gauge observations at stations Quarry Bay $H_{\rm Q}(t)$, ShekPik $H_{\rm S}(t)$ and Waglan Island $H_{\rm W}(t)$ respectively. From this figure, we can see several data gaps induced by the failures of the recording system, among them one gap is found at station Quarry Bay (30h in total), eight gaps are found at station ShekPik (463h in total) and fourteen gaps are found at station Waglan Island (2329h in total), the longest gap is from July 23, 2003 to September 19, 2003 (1386h in total). In addition, from Fig. 5, the tidal amplitude in the near sea of Hongkong area reaches to a magnitude of 3m during this period. The tricubic polynomial is used to fit the characteristics of the long term change in tidal height, the analysis shows that this change correlates closely to the local sea level change. The following analysis demonstrates also that due to the uncertainty of the global ocean models in shallow seas, it is very important to consider the tide gauge data in the investigation of station background noise. To carry out the preprocessing of the tidal gauge data, various recording errors as electronic pulses and so on are removed with an interactive visual screen. Finally, the tide gauge data are arranged into the same format files with those in tidal gravity and air pressure data for further analysis.

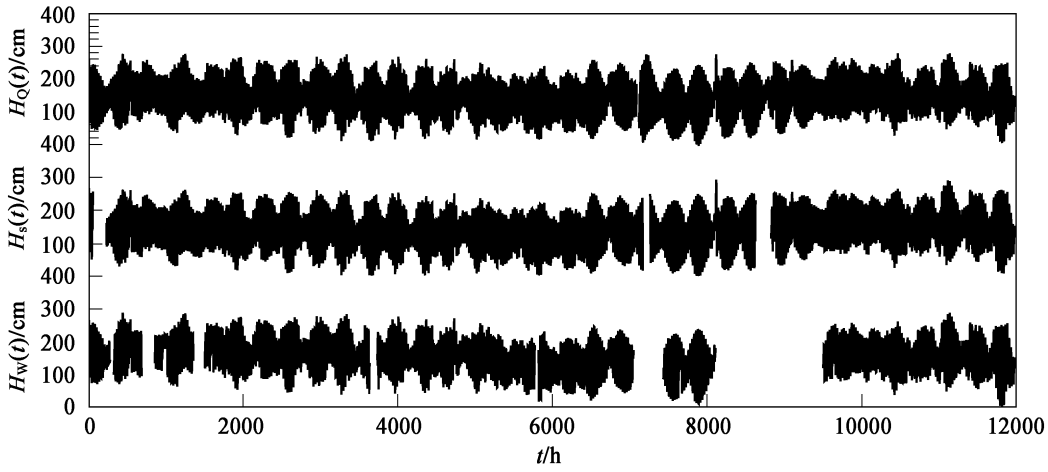

Fig. 5 Tidal variation at tidal gauge stations Quarry Bay $H_{\rm Q}(t)$ (a), ShekPik $H_{\rm S}(t)$ (b) and Waglan Island $H_{\rm W}(t)$ (c)

3 ANALYSIS OF THE GRAVITY TIDE DATA

3.1 Determination of the Tidal Parameters

After having the corrected 1h sampling tidal gravity and air pressure observations, the tidal gravity parameters can be estimated. During the procedure in the estimation of tidal parameters, considering the characteristics of the different angular frequencies for various waves and the certain property of the specific odd even band filters, the diurnal (D), semidiurnal (SD), tri-diurnal (TD)wave groups are separated from the tidal gravity signals after removing the drift term from observations[13]. In the geophysical point of view, the tidal gravity signal can be separated into the combination of various wave groups. Strictly specking, to those waves with almost similar angular frequency, the Love number is different. However, for the reason that the difference of wave angular frequencies in one wave group is comparatively very small, the Love numbers in one wave group can be regarded as a constant in the data harmonic analysis.

The second step in the data analysis is to solve corresponding tidal gravity observation equations with the classical Least Square method and to estimate tidal parameters of various wave groups (including amplitude factors and phase lags) and their corresponding standard errors. The observed tidal gravity residuals are calculated by deducting the theoretical tidal signals from observed tidal gravity signals in both time and frequency domains. The regression coefficient (i.e., the atmospheric gravity admittance) is calculated by using the regression technique between the tidal gravity residual and the station air pressure. The residual amplitude spectrum is obtained by carrying out the spectral analysis to tidal gravity residual series. The mean standard deviation (i.e., noise level) for each of the tidal frequency band is also estimated. In the data analysis, the tidal potential expansion table with 12000 tidal components recommended by the International Earth Tides Commission (IETC) is employed[14].

The tidal gravity parameters in Hongkong region are calculated by using the standard Eterna packages given by Wenzel in Karlsruhe University, Germany and recommended by the ICET[11]. Table 1 shows the amplitude factors, phase lags and the corresponding error estimation for 17 waves in D, 13 waves in SD and 1 wave in TD bands. The names of the wave groups and their beginning and ending frequency are also shown in

Table 1 The observed tidal parameters at station in Hongkong (corrected for station air pressure effect)

Wave name	Beginning frequency	Ending frequency	Amplitude factor	Standard deviation	Phase lag (°)	Standard deviation (°)
SGQ_1	0.721499	0.833113	1.20922	0.05955	–8.2171	2.8229
$2Q_1$	0.851181	0.859691	1.20314	0.02008	–2.1549	0.9585
SGM_1	0.860895	0.870024	1.18700	0.01730	–3.7940	0.8353
Q_1	0.887326	0.896130	1.22450	0.00281	–4.2680	0.1316
RO_1	0.897806	0.906316	1.21511	0.01529	–4.1587	0.7200
O_1	0.921940	0.930450	1.20270	0.00059	–4.9480	0.0278
TAU_1	0.931963	0.940488	1.28978	0.06048	–1.3680	2.6869
NO_1	0.958085	0.966757	1.16940	0.00630	–5.1746	0.3084
CHI_1	0.968564	0.974189	1.12129	0.03919	–4.6413	2.0032
P_1	0.989048	0.998029	1.13942	0.00166	–4.6377	0.0847
S_1	0.999852	1.000148	1.00650	0.13049	57.0101	6.0177
K_1	1.001824	1.013690	1.12347	0.00050	–4.3523	0.0253
TET_1	1.028549	1.034468	1.14447	0.03863	–3.1539	1.9357
J_1	1.036291	1.044801	1.14594	0.00732	–2.8634	0.3661
SO_1	1.064840	1.071084	1.19459	0.04314	–3.6087	2.0699
OO_1	1.072582	1.080945	1.12122	0.00970	–1.2241	0.4950
NU_1	1.099160	1.216398	1.18899	0.04537	0.9368	2.1868
EPS_2	1.719380	1.837970	1.22822	0.03033	–0.3920	1.4149
$2N_2$	1.853919	1.862429	1.20963	0.01047	–2.4906	0.4960
MU_2	1.863633	1.872143	1.20157	0.00852	–1.4034	0.4061
N_2	1.888386	1.896749	1.18533	0.00135	–2.1325	0.0655
NU_2	1.897953	1.906463	1.16312	0.00701	–1.4449	0.3453
M_2	1.923765	1.942754	1.17608	0.00025	–2.0243	0.0123
LAM_2	1.958232	1.963709	1.15104	0.03469	–1.0334	1.7258
L_2	1.965826	1.976927	1.17313	0.00765	–1.2295	0.3736
T_2	1.991786	1.998288	1.17812	0.00997	0.1012	0.4909
S_2	1.999705	2.000767	1.16432	0.00067	–2.1494	0.0486
K_2	2.002590	2.013690	1.17331	0.00168	–1.8731	0.0830
ETA_2	2.031287	2.047391	1.12779	0.02760	–1.2779	1.4025
$2K_2$	2.067578	2.182844	1.17794	0.06257	–2.5692	3.0425
M_3	2.753243	3.081255	1.06012	0.00437	–1.7495	0.2362

this table. The numerical results demonstrate that the amplitude of the main tidal waves in Hongkong area can reach to 26.2×10^{-8}m·s^{-2} for O_1 wave, 34.4×10^{-8}m·s^{-2} for K_1 wave, 75.6×10^{-8}m·s^{-2} for M_2 wave and 34.8×10^{-8}m·s^{-2} for S_2 wave; and the average standard deviation of the tidal amplitude is 0.4×10^{-8}m·s^{-2}. The accuracy of the amplitude factors of the main waves reaches to 0.6‰ for O_1 wave, 0.5‰ for K_1 wave, 0.3‰ for M_2 wave and 0.7‰ for S_2 wave. The accuracy of the phase lags for the main waves is 2.8% for O_1 wave and 1.2% for M_2 wave. These numerical results declare that high-accuracy gravity tide parameters in Hongkong are obtained with the LCR-ET20 gravimeter. From Table 1, it is found that, generally speaking, the determined phase lags are comparatively large. The following analysis shows that it is mainly induced by the ocean tide. Furthermore, the phase lag of the S_1 wave is as high as 57° and appearing as a leading phenomenon, it is mainly related to the particular meteorological factors in Hongkong area.

3.2 Ocean Loading Correction

With the wide use of the satellite altimetry techniques and the continuous development of the finite element method, many new global ocean models are published in recent years. 11 various global digital ocean tidal models in total are used in this study, including the AG95 (Andersen, 1995), CSR3.0 (Eanes, 1996), CSR4.0 (Eanes, 1999), FES95.2 (Le Provost, 1994), FES99 (Lefèvre, 2000), FES02 (Lefèvre, 2002), GOT00 (Ray, 1999), NAO99 (Matsumoto, 2000), ORI96 (Matsumoto, 1996), TPXO2 (Egbert, 1994), and SCW80 (Schwiderski, 1980)[15~25]. Due to the difference of the used methods, satellite orbit data, and tide gauge data in the construction of the global ocean models, they induce certain discrepancy among the ocean models. Therefore the results of the tidal gravity observations can be used to check the global ocean models. As a result, we can find the suitable models in this area and provide effective reference to the geodesy, oceanography, and space geodesy techniques.

Generally, the global ocean models provide us comparatively high precision amplitude and phase of the ocean tides in the open sea area. However, even the finest global ocean model cannot still describe accurately the motion characteristics of the costal tides because of the complex coast, the specific tectonics of the sea floor and the large gradient of the tide change in Chinese near seas. Therefore, the coastal tidal data of China seas must be taken into account in the investigation of the tidal gravity loading effect[26]. The newest digital grid ocean maps of four main waves (O_1, K_1, M_2 and S_2 waves) developed by Institute of Oceanography, Chinese Academy of Sciences are used to modify effectively the global ones[27]. They are the ocean maps of the southern China sea area (latitude from 1°45′N to 25°15′N, and longitude from 99°E to 121°30′E, grid interval $15'\times15'$) and of the eastern China sea area (latitude from 23°50′N to 41°N, and longitude from 117°30′E to 131°30′E, grid interval $10'\times10'$).

After having the grid digital ocean models, the gravity loading vectors can be then calculated. According to the technique of integrated Green's function developed by Agnew[28], the gravity loading vectors of the main waves are then calculated, separately. The gravity loading corrections are carried out based on the vector superposition principle[29,30]. Fig. 6 represents the comparison of the amplitudes of the ocean loading vectors for four main waves. The numerical results demonstrate that in the D frequency band, the loading amplitude of O_1 wave is 2.0×10^{-8}m·s^{-2} and the corresponding phase is 53.5°, the amplitude difference of the ocean loading vectors of O_1 wave obtained from different ocean models is 6% and the largest difference of the phase is 2°. In the SD frequency band, the loading amplitude of M_2 wave is 1.9×10^{-8}m·s^{-2}, and the discrepancy of the loading amplitude obtained from different ocean models is 8%, the largest discrepancy of the phase difference is 8°.

When taking different global ocean models, the loading amplitudes of K_1 and O_1 waves in the D frequency band are of the same magnitude, but the difference of the loading amplitude of the waves in the SD frequency band is comparatively large. For example, the loading amplitude of S_2 wave is $0.6t\times10^{-8}$m·s^{-2}, which is much smaller than that of M_2 wave. This reflects the changing characteristics of the different waves. Further analysis indicates that for a certain wave, comparing the loading results obtained when using global ocean models and those modified by local ones, it is found that the loading discrepancy is mainly induced by the uncertainty of the local models. Therefore, it is extremely important to take this factor into account in the determination of the resonance parameters of the Earth's liquid core and inversion for the structure of the Earth's interior[31].

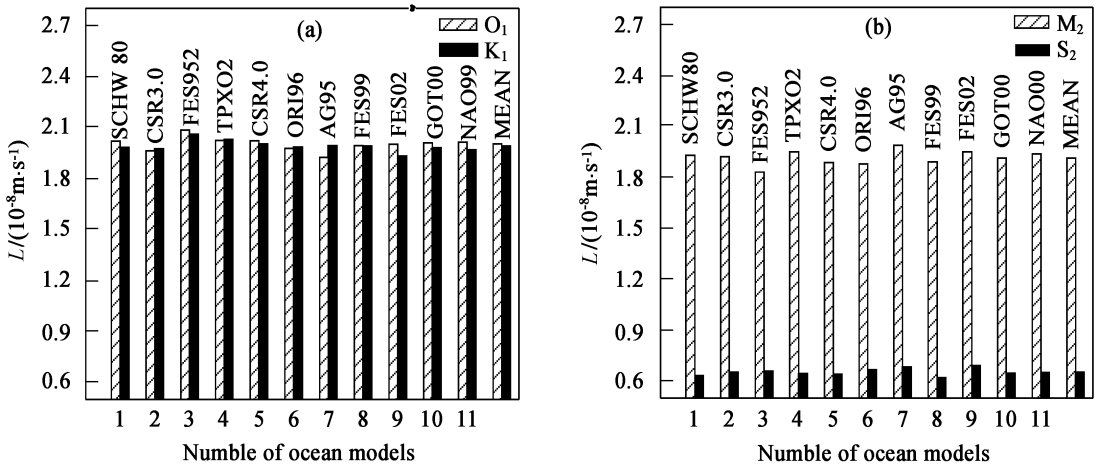

Fig. 6 Amplitudes of gravity loading vectors for main constituents in diurnal (a) and semidiurnal (b) bands

Based on the gravity loading results obtained using 11 various ocean models, the ocean loading correction is carried out on tidal gravity parameters. Table 2 shows the comparison of the residual vectors for four main waves before and after loading correction using various ocean models. From this table it is known that the residual amplitude decreases significantly after loading correction. Averaging the gravity residual results after loading correction with 11 ocean models, it is found that the residual amplitude of O_1 wave is decreased from $1.89\times10^{-8}\mathrm{m\cdot s^{-2}}$ to $0.43\times10^{-8}\mathrm{m\cdot s^{-2}}$, that of K_1 wave is decreased from $2.06\times10^{-8}\mathrm{m\cdot s^{-2}}$ to $0.10\times10^{-8}\mathrm{m\cdot s^{-2}}$, that of M_2 wave is decreased from $2.11\times10^{-8}\mathrm{m\cdot s^{-2}}$ to $0.66\times10^{-8}\mathrm{m\cdot s^{-2}}$, and that of S_2 wave is decreased from $1.04\times10^{-8}\mathrm{m\cdot s^{-2}}$ to $0.39\times10^{-8}\mathrm{m\cdot s^{-2}}$.

Table 2 Comparison of the residual vector among the four main waves after the tidal loading correction with different ocean models

Waves	O_1 wave			K_1 wave		M_2 wave		S_2 wave	
	$X/(10^{-8}\mathrm{m\cdot s^{-2}})$	$\chi/(°)$		$X/(10^{-8}\mathrm{m\cdot s^{-2}})$	$\chi/(°)$	$X/(10^{-8}\mathrm{m\cdot s^{-2}})$	$\chi/(°)$	$X/(10^{-8}\mathrm{m\cdot s^{-2}})$	$\chi/(°)$
$\boldsymbol{B}$(Obs)	1.8929	–65.80		2.0562	–93.79	2.1121	–67.33	1.0353	–77.90
$\boldsymbol{X}_1$(SCW80)	0.4688	–164.69		0.0992	–53.34	0.5046	–129.46	0.4035	–77.97
$\boldsymbol{X}_2$(CSR3.0)	0.4242	–158.83		0.1230	–47.50	0.6835	–131.90	0.3850	–83.31
$\boldsymbol{X}_3$(FES95.2)	0.4229	–177.06		0.0309	2.17	0.7204	–124.83	0.4025	–93.81
$\boldsymbol{X}_4$(TPX02)	0.4157	–168.22		0.1147	–18.94	0.7540	–134.61	0.4047	–89.44
$\boldsymbol{X}_5$(CSR4.0)	0.4265	–167.04		0.1023	–36.99	0.5507	–126.18	0.3939	–77.10
$\boldsymbol{X}_6$(OR196)	0.4312	–160.48		0.1000	–50.64	0.8035	–129.66	0.4024	–96.79
$\boldsymbol{X}_7$(AG95)	0.4287	–153.31		0.1085	–40.88	0.6122	–137.29	0.3533	–79.24
$\boldsymbol{X}_8$(FES99)	0.4028	–164.38		0.1133	–40.27	0.5512	–126.42	0.4158	–78.84
$\boldsymbol{X}_9$(FES02)	0.4615	–162.58	0.1575		–57.65	0.6951	–134.26	0.3495	–86.51
$\boldsymbol{X}_10$(GOT00)	0.4311	–165.12	0.0980		–55.37	0.6800	–131.23	0.3897	–82.31
$\boldsymbol{X}_11$(NAO99)	0.4536	–164.54	0.1027		–64.53	0.6915	–133.33	0.3952	–87.92
$\boldsymbol{X}_12$(EMAN)	0.4313	–164.17		0.1013	–45.60	0.6574	–130.97	0.3881	–84.88

Note: X is the amplitude ($10^{-8}\mathrm{m\cdot s^{-2}}$) and χ is the phase (°). $\boldsymbol{B}$(Obs) is the observed residual vector, $\boldsymbol{X}_1(SCW80)$, $\boldsymbol{X}_2(CSR3.0)$, ···, $\boldsymbol{X}_11(NAO99)$ are the final residual vectors after the ocean loading correction with different ocean models. $\boldsymbol{X}_12$(EMAN) is the average residual vector of all the 11 ocean models. The words in the brackets denote the name of the corresponding ocean model.

In order to evaluate comprehensively the loading correction, the concept of "loading correction efficiency" is introduced here, i.e., the difference of the amplitude between observed and final residual vectors divided by the observed residual amplitude. The aim of this concept is to determine the adaptability of the global ocean

models in Hongkong area[30]. As an example, Fig. 7 shows the statistics of the loading correction efficiency for two D waves (O_1 and K_1) and for two SD waves (M_2 and S_2). In general, the loading correction efficiency in the D wave band is higher than that in the SD wave band. Among them, the most obvious one is K_1 wave, the efficiency reaches as high as 98.50% (FES95.2), and the lowest one is the S_2 wave, the efficiency is 59.84% (FES99). The average loading correction efficiency for 11 global models is 77.2% (O_1 wave), 95.1% (K_1), 68.8% (M_2 wave) and 62.5% (S_2 wave). The analysis of the results shows that the difference of the loading correction efficiency reflects the discrepancy of the different ocean models. Higher loading correction efficiency corresponds to the more complete ocean loading correction, and then the ocean model is more suitable at this area. Therefore, to the O_1 wave, the influence of using different ocean models to the result is very small, it means that the result after various ocean loading correction is almost the same. But to the M_2 wave, the case is quite different, the discrepancy of the efficiency of the loading correction is relatively large. The relatively higher efficiency results from CSR4.0 model (73.9%), and the relatively lower efficiency is from FES95.2 model (64.3%), the difference between them is as high as 13%.

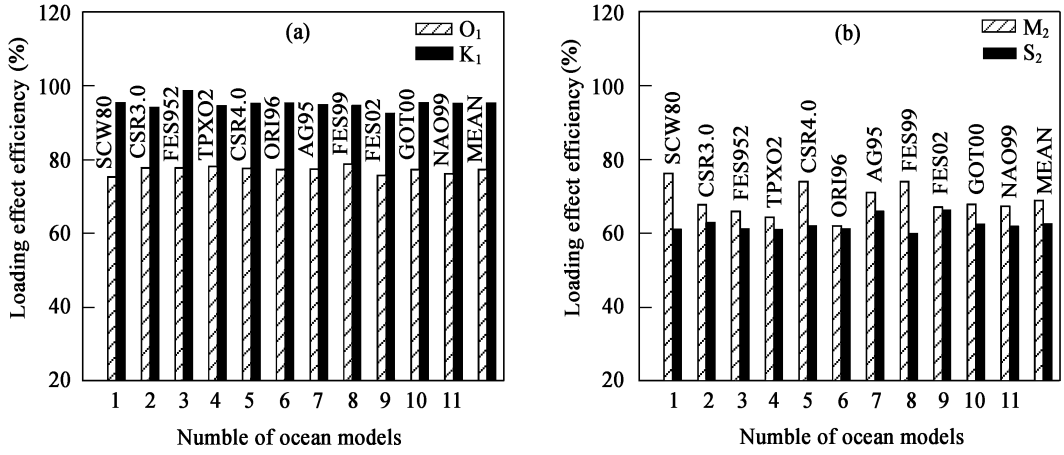

Fig. 7 Loading correction efficiency of amplitude factors for main constituents in diurnal (a) and semidiurnal (b) bands

There are relatively large errors in the local ocean tidal models, because they are constructed by interpolation based on the hydrodynamic equation, taking into account the limited tidal gauge observations as constraints, and the bay terrain in Hongkong area is complex. Therefore, in order to compensate the uncertainty of the local models in Hongkong area, the changes in tidal level recorded at tide gauge station are taken into account. In the practical processing, the regression analysis between the tidal gravity residual and sea level change series is carried out to obtain regression coefficient. Using this regression coefficient, the loading effect is further deducted from the observed tidal gravity residuals. The regression coefficients determined are $0.017 \pm 0.006 \times 10^{-8} \mathrm{m \cdot s^{-2}/cm}$ for station Quarry Bay, $0.016 \pm 0.007 \times 10^{-8} \mathrm{m \cdot s^{-2}/cm}$ for station ShekPik and $0.018 \pm 0.009 \times 10^{-8} \mathrm{m \cdot s^{-2}/cm}$ for station Waglan Island respectively. The numerical results demonstrate that after considering the tidal gauge observations, the accuracy of the tidal gravity parameters is improved significantly in the D and SD bands. The corrections are done respectively using 3 tidal gauge series, and the best one is chosen. It shows that the largest difference of the standard deviation of tidal gravity is at the level of 3%.

Taking the tidal gauge series at station Quarry Bay as an example, Table 3 shows the numerical results of the two D waves and two SD waves. In Table 3, column I gives the tidal gravity parameters after station air pressure correction. Column II gives those after the corrections of station air pressure and the NAO99 global ocean tide model (modified by the local ones). Column III gives those after the further correction of the tide gauge data on the results in column II. From the table, we can see that after correction of the tide gauge data, the tidal gravity amplitude factors have a difference of 1% comparing to those before the correction, the phase lags are improved obviously. It shows the importance of the correction of the local ocean tidal height.

Table 3 shows also the amplitude factors of the DDW2 theoretical Earth tide model under the non-hydrostatic equilibrium status[31]. The comparison demonstrates that after the ocean loading correction, the discrepancy between the observed amplitude factors and theoretical ones decreases from 4.2% to 1.0% for O_1 wave, from 1.2% to 0.6% for M_2 wave. The decrease of the phase lag is significant, from –4.95° to –1.51° for O_1 wave, from –4.35o to –1.08o for K_1 wave, from –2.02° to –0.94° for M_2 wave, and from –2.15° to –1.14° for S_2. After taking the tide gauge data into account, the phase lags are further improved, from –1.51° to –0.28° for O_1 wave, form –1.08° to –0.15° for K_1 wave, from –0.94° to –0.39° for M_2 wave, and from –1.14o° to –0.65° for S_2 wave. It indicates that the correction of the tidal height variation on the tidal gravity parameters is significant, especially to the phase lags. The corrections of the near sea level change data from ShekPik and Waglan Island are also carried out respectively, and the results show the difference among the corrected tidal gravity parameters when using different tide gauge series is relatively slight.

Table 3 Tidal gravity parameters after loading corrections of the NAO99 model and tide gauge data at station Quarry Bay

Station	Waves	I		II		III		Theoretical
		Amp. Fac.	Phase lag(°)	Amp. Fac.	Phase lag(°)	Amp. Fac.	Phase lag(°)	Amp. Fac.
Qarry Bay	O_1	1.2027	–4.95	1.1429	–1.51	1.1342	–0.28	1.1542
	K_1	1.1235	–4.35	1.1263	–1.08	1.1363	–0.15	1.1349
	M_2	1.1761	–2.02	1.1554	–0.94	1.1544	–0.39	1.1618
	S_2	1.1643	–2.15	1.1569	–1.14	1.1623	–0.65	1.1618

Note: Column I gives tidal gravity parameters after air pressure correction; Column II gives those after corrections of air pressure and of the NAO99 global ocean tide model. Column III gives those after further correction of tide gauge data on results given in column II. "Amp. Fac." is the abbreviation of "amplitude factor".

3.3 Time Analysis of the Gravity Residual

The synthesized tidal gravity signals $S(t)$ in Hongkong area are reconstructed according to the observed tidal gravity parameters given in Table 1. Then the irregular long term tidal gravity residual $R(t)$ is obtained by deducting the synthesized signals from the observations (Fig. 8b). From the figure we can see that the drift term in gravity residual is still very large although we have get rid of the long term drift by using the polynomial fit technique. The peak to peak change is about $200\times10^{-8}\mathrm{m\cdot s^{-2}}$. In order to investigate the station background noise level, the gravity residuals are filtered by using a least square high-pass filter with cut-off frequency of 0.8 cpd. The filtered residual $R_{\mathrm{f}}(t)$ is shown as Fig. 8. In order to show the efficiency in the temporal domain, the corrections of the air pressure and of the tide gauge sea level of Quarry Bay are carried out respectively. The gravity residual after air pressure correction $R_{\mathrm{fp}}(t)$, and the gravity residual after correction of the tide gauge data of Quarry Bay $R_{\mathrm{ft}}(t)$ are given in Fig. 8, it is found that the influence of the air pressure on gravity residual is very small (this case is also shown clearly in Fig. 9). However, after the correction of local sea level data, the amplitude of the residual gravity decreases significantly, it shows that the influence of shallow ocean tides on tidal gravity observation is obvious, it can be seen that the station background noise level is at about $\pm2.0\times10^{-8}\mathrm{m\cdot s^{-2}}$ level. On the other hand, the analysis shows that the influence of the local ocean tide is also at about $\pm2.0\times10^{-8}\mathrm{m\cdot s^{-2}}$. Consequently, if the accurate tidal gravity parameters are required, the change in tidal height in near ocean should be taken into account.

For obtaining the signals of shallow sea tide in tidal gravity residual, the spectral characteristics of the tidal gravity residual is also investigated in frequency domain. By carrying out the Fast Fourier Transform (FFT) algorithm with the Hanning window to three gravity residual series ($R_{\mathrm{f}}(t)$, $R_{\mathrm{ft}}(t)$ and $R_{\mathrm{fp}}(t)$) given in Fig. 8, the spectral residual amplitudes (A_{f}, A_{fp} and A_{ft}) are obtained respectively (Fig. 9). From the analysis, it is found that the difference between A_{f} and A_{fp} is very small. However, comparing A_{fp} and A_{ft}, it is found that the residual amplitude of the tidal gravity decreases significantly. In the D frequency band, more than 90%

of the final residual signals disappeared due to applying the correction of local sea level data. In the SD tidal band, the residual amplitude decreases from $0.50\times10^{-8}\mathrm{m\cdot s^{-2}}$ to $0.15\times10^{-8}\mathrm{m\cdot s^{-2}}$, the effect is very significant. It shows the influence of the variation of the local tidal height to be $0.35\times10^{-8}\mathrm{m\cdot s^{-2}}$.

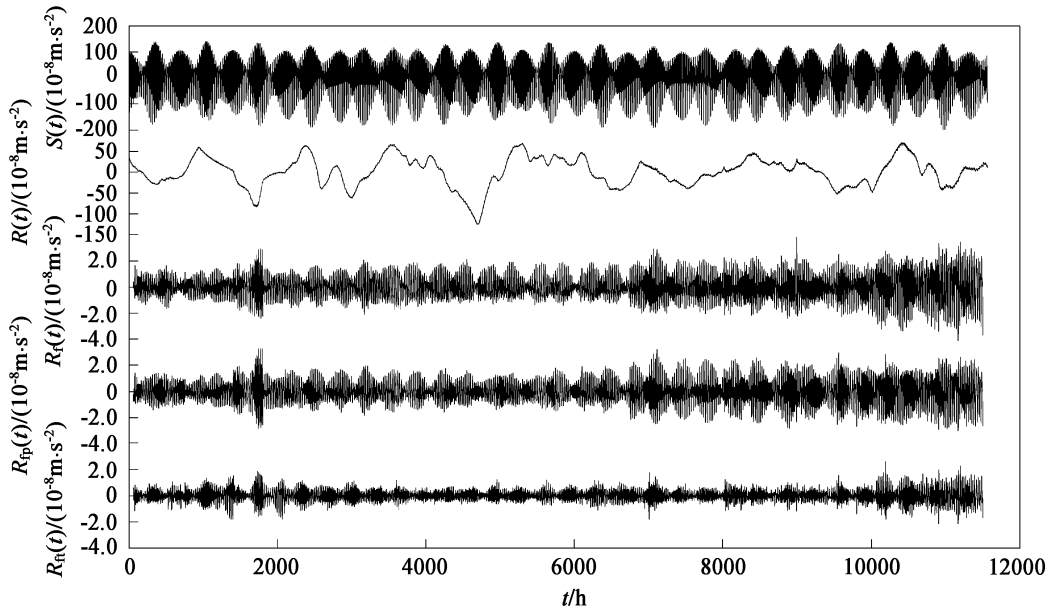

Fig. 8 Synthesized tidal gravity $S(t)$, irregular long period gravity change $R(t)$, tidal gravity residual tidal gravity residual after air pressure correction ($R_{\mathrm{f}}(t)$ and tidal gravity residual after air pressure $R_{\mathrm{fp}}(t)$ and tidal gauge data corrections $R_{\mathrm{ft}}(t)$

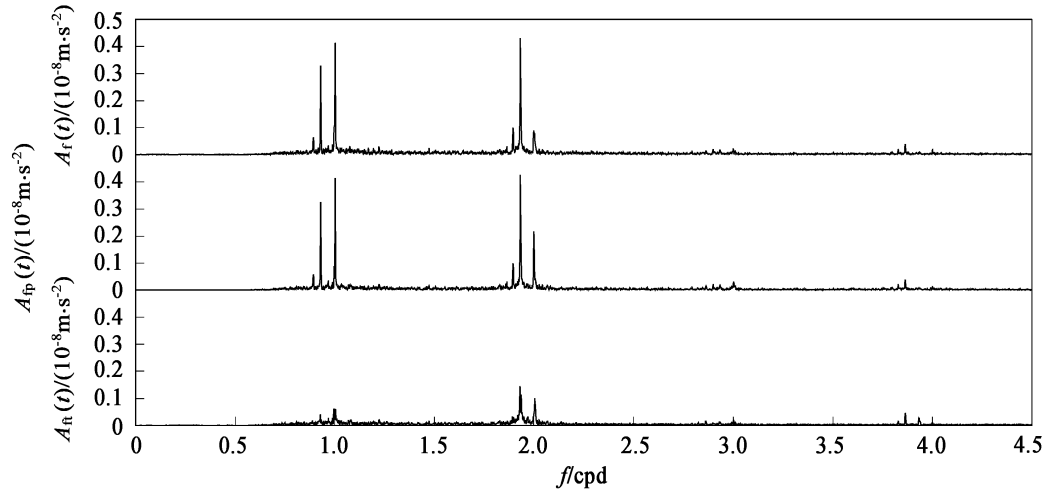

Fig. 9 Spectrum amplitudes of tidal gravity residual signals, original $A_{\mathrm{ft}}(t)$, after air pressure correction $A_{\mathrm{ft}}(t)$ and after air pressure and tidal gauge data corrections $A_{\mathrm{ft}}(t)$

4 CONCLUSIONS

Based on the numerical results and discussion mentioned above, the following conclusions can be drawn:

(1) The complete experimental tidal gravity model in Hongkong area is accurately obtained for the first time by using the observations of high precision gravimeter for a period of 483 days. Our study has filled the empty of tidal gravity observation in this area in the Crustal Movement Observation Network of China and can provide the effective reference and service to the ground surface and space geodesy;

(2) The gravity loading vectors are calculated based on the 11 various global ocean models modified by the local sea maps. The loading correction on tidal gravity parameters is carried out. The results demonstrate that the amplitudes of the residual vectors are improved obviously, and the average efficiency of the loading correction is as high as 77.2% (O_1 wave), 95.1% (K_1), 68.8% (M_2 wave) and 62.5% (S_2 wave). The discrepancies between the observed tidal gravity amplitude factors and the theoretical ones are decreased significantly after ocean loading correction;

(3) The adaptability of the ocean models in Hongkong area is discussed in this paper. It shows that the influence of different ocean models in the D wave band is very small. However, in the SD wave band, the difference of the loading correction efficiency is as high as 13% when adopting different ocean models. That is to say, the ocean models in the D frequency band are more stable than those in the SD frequency band;

(4) The observed gravity residual and station background noise level are also studied by using tide gauge observations. The result shows that the background noise of tidal gravity observations in Hongkong area is at the same level with those induced by the costal shallow sea tides. The phase lags of the tidal parameters for main waves are improved significantly after coastal shallow sea tides correction. Therefore, it is a valid compensation to take the tidal gauge data into account in considering large error of the local ocean models due to the complex bay terrain in Hongkong area.

ACKNOWLEDGMENTS

The authors would like to give their gratitude to Mr. Wong WT in Hongkong Astronomy Observatory in help us to manage observation room. This research is supported jointly by the Hundred Talents Program, the knowledge innovation Project of Chinese Academy of Sciences (Grant No. KZCX3-SW-131), the Natural Sciences Foundation of China (Grant No. 40374029), the Hong Kong Research Grant Council (PolyU 5075/01E), and the Hong Kong Polytechnic University (A-PD51).

REFERENCES

[1] Fang J. Earth Tides (in Chinese). Beijing: Science Press, 1984

[2] Crossley D, Hinderer J, Casula G, et al. Network of superconducting gravimeters benefits a number of disciplines. *Eos, Tran.*, American Geophysical Union, 1999, **80**(11): 121125∼121126

[3] Sun H P, Hsu H Z, Jentzsch G, et al. Tidal gravity observations obtained with superconducting gravimeter and its application to geodynamics at Wuhan/China. *Journal of Geodynamics*, 2002, **33**(1-2): 187∼198

[4] Sun H P, Xu J Q, Ducarme B. Experimental earth tidal models in considering nearly diurnal free wobble of the Earth's liquid core. *Chinese Science Bulletin*, 2003, **48**(9): 935∼940

[5] Melchior P. A new data bank for tidal gravity measurements (DB92). *Phys. Earth Planet. Inter.*, 1994. **82**: 125∼155

[6] Ducarme B, Sun H P. Tidal gravity results from GGP network in connection with tidal loading and earth response. *J. Geodetic Society of Japan*, 2001, **47**(1): 308∼315

[7] Becker E, Groten E, Tao G X, et al. An improved ET Earth tide gravimeter. *Acta Geodaetica et Cartographic Sinica* (in Chinese), 1990, **19**(3): 229∼235

[8] Liu M, Sun H P, Zheng S H, et al. Data acquisition and display system of LaCoste-Romberg ET gravimeter based on visual instrument. *Electronic Measurement Technology* (in Chinese), 2002, **6**: 38∼40

[9] Sun H P, Chen X D, Liu M, et al. Analysis and comparison of the tidal gravity observations obtained with LCR-ET20 spring gravimeter. *Acta Seismologica Sinica* (in Chinese), 2002, **24**(5): 510∼515

[10] Vauterin P. Tsoft: Graphical and interactive software for the analysis of Earth tide data. Proc. 13th Int. Sympos. on Earth Tides, Brussels, Observatoire Royal de Belgique, Série Géophysique, 1998. 481∼486

[11] Wenzel H G. The Nanogal Software: Earth tide data processing pakage Eterna3.30. *Bulletin d'Information de Marees Terrestres*, 1996, **124**: 9425∼9439

[12] Chen X D, Sun H P. New method for pre-processing and analyzing tidal gravity observations. *Journal of Geodesy and Geodynamics* (in Chinese), 2002, **22**(3): 83∼87

[13] Sun H P, Takemoto S, Hsu H T, et al. Precise tidal gravity recorded with superconducting gravimeters at stations Wuhan/China and Kyoto/Japan. *J. Geodesy*, 2001, **74**: 720∼729

[14] Hartmann T, Wenzel H G. The HW95 tidal potential catalogue. *Geophys. Res. Lett.*, 1995, **24**: 3553∼3556

[15] Andersen O B. Global ocean tides from ERS1 and TOPEX/Poseidon. *J. Geophys. Res.*, 1995, **100**: 25249∼25259

[16] Eanes R J, Shuler A. An improved global ocean tide model from TOPEX/Poseidon altimetry: CSR4.0. EGS 24th General Assembly, The Hague, 1999

[17] Eanes R J, Bettadpur S V. The CSR3.0 global ocean tide model. CSR- TM- 95- 06, Center for Space Research, Univ. of Texas at Austin, 1995

[18] Le Provost C, Lyard F, Molines J M, et al. A hydrodynamic ocean tide model improved by assimilating a satellite altimeter-derived data set. *J. Geophys. Res.*, 1998, **103**(C3): 5513∼5529

[19] Lefèvre F, Lyard F, Le Provost C, et al. FES99: a global tide finite element solution assimilating tide gauge and altimetric information. *J. A. O. T.*, 2002, **19**: 1345∼1356

[20] Le Provost C. FES2002-A new version of the FES tidal solution series. Abstract Volume. Jason-1 Science Working Team Meeting, Biarritz, France, 2002

[21] Ray R. A global ocean tide model from TOPEX/Poseidon altimetry: GOT99.2. Goddard Space Flight Center/NASA, Greenbelt, TM-1999-209478, 1999. 58

[22] Matsumoto K, Ooe M, Sato T, et al. Ocean tide model obtained from TOPEX/Poseidon altimetry data. *J. Geophys. Res.*, 1995, **100**: 25319∼25330

[23] Matsumoto K, Takanezawa T, Ooe M. Ocean tide models developed by assimilating TOPEX/POSEIDON altimeter data into Hydro-dynamical model: A global model and a regional around Japan. *Journal of Oceanography*, 2000, **56**: 567∼581

[24] Egbert G D, Bennett A F, Foreman M G G. TOPEX/POSEIDON tides estimated using a global inverse model. *J. Geophys. Res.*, 1994, **99**: 24821∼24852

[25] Schwiderski E W. Ocean tides, Part II: A hydrodynamical interpolation model. *Marine Geodesy*, 1980, **3**: 219∼255

[26] Sun H P. Comprehensive researches for the effect of the ocean loading on gravity observations in the Western Pacific Area. *Bulletin d'informations de Marees Terrestres*, 1992, **113**: 8271∼8292

[27] Fang G H, Kwok Y K, Yu K, et al. Numerical simulation of principal tidal constituents in the South China Sea, Gulf of Tonkin and Gulf of Thailand. *Continental Shelf Research*, 1999, **19**(7): 845∼869

[28] Agnew D C. A program for computing ocean-tide loading. *J. Geophys. Res.*, 1997, **102**(B3): 5109∼5110

[29] Sun H P, Hsu H Z, Luo C S, et al. Study of the ocean models using tidal gravity observations obtained with superconducting gravimeter. *Acta Geodaetica et Cartography Sinica* (in Chinese), 1999, **28**(2): 115∼120

[30] Sun H P, Ducarme B, Xu H Z et al. Adaptability of the ocean and Earth tidal models based on global observations of the superconducting gravimeters. *Science in China* (Sereis D): Earth Science, 2005, **48**(11): 1859∼1869

[31] Dehant V, Defraigne P, Wahr J. Tides for a convective Earth. *J. Geophys. Res.*, 1999, **104**(B1): 1035∼1058